Chinese Chemical Letters 35 (2024) 109742

Contents lists available at ScienceDirect

Chinese Chemical Letters

journal homepage: www.elsevier.com/locate/cclet

Active-transporting of charge-reversal Cu(II)-doped mesoporous silica nanoagents for antitumor chemo/chemodynamic therapy

Zhaomin Tang[a,*], Qian He[a], Jianren Zhou[a], Shuang Yan[a], Li Jiang[a], Yudong Wang[a], Chenxing Yao[b], Huangzhao Wei[b,*], Keda Yang[c,*], Jiajia Wang[d,*]

[a] School of New Energy and Materials, Southwest Petroleum University, Chengdu 610500, China
[b] Dalian Institute of Chemical Physics, Chinese Academy of Sciences, Dalian 116023, China
[c] Shulan International Medical College, Zhejiang Shuren University, Hangzhou 310015, China
[d] Department of Laboratory Medicine, Sichuan Provincial People's Hospital, University of Electronic Science and Technology of China, Chengdu 610072, China

ARTICLE INFO

Article history:
Received 28 November 2023
Revised 2 March 2024
Accepted 6 March 2024
Available online 15 March 2024

Keywords:
Cu(II)-doped
Ascorbate
Hydrogen peroxide
Charge-reversal
Oxidative damage

ABSTRACT

Fe-based Fenton agents can generate highly reactive and toxic hydroxyl radicals (·OH) in the tumor microenvironment (TME) for chemodynamic therapy (CDT) with high specificity. However, the low pH environment and insufficient endogenous hydrogen peroxide (H_2O_2) of the highly efficient Fenton reaction limits its practical application in clinic. Here, a Cu(II)-doped mesoporous silica nanoagent (Cu-MSN) with excellent dispersity was successfully developed. After loaded with doxorubicin (DOX) and ascorbate (AA), Cu-MSN@DA was coated with active targeting ligand folic acid (FA), dimethyl maleic an-hydride (DMMA) and carboxymethyl chitosan (CMC) to obtain an active transporting nanoagent (FCDC@Cu-MSN@DA) with tunable charge-reversal property, which is more adaptable to the pH value of TME than Fe-based Fenton agents, and can self-supply exogenous H_2O_2 by ascorbate to produce more toxic ·OH to trigger the apoptosis of cancer cells. Meanwhile, the high level of glutathione (GSH) in TME can reduce Cu(II) to Cu(I) by Fenton-like reaction, increasing the generation rate of ·OH and relieving tumor antioxidant ability. The supply of exogenous H_2O_2 significantly enhanced the synergistic effect of CDT by oxidative damage. Together with DOX-induced cell apoptosis, this novel nanoagent FCDC@Cu-MSN@DA can achieve maximum therapeutic efficacy, creating a new model of safe and effective tumor treatment with high specificity.

Cancer has become the predominant cause of death in the world today [1,2]. Traditional chemotherapy is the principal method against cancer in clinic. However, its curative effect is often unsatisfactory due to the intrinsic resistance of tumor cells to apoptosis [3]. The production of highly cytotoxic reactive oxygen species (ROS) by versatile nanoplatform has been considered as a promising strategy for promoting cancer cellular necrosis or apoptosis [4]. In particular, ROS-involved chemodynamic therapy (CDT) based on highly toxic ·OH generated *via* Fenton or Fenton-like reaction has been developed rapidly in recent years [4–6]. The nanoagents consisted of transition metal (Fe, Cu, Mn, Co) have exhibited outstanding efficacy to generate toxic hydroxyl radical (•OH) from tumoral H_2O_2 by CDT [7].

Copper is an essential mineral nutrient that is widespreadly necessary for various physiological processes, including mitochondrial respiration, oxidative phosphorylation, biomolecule synthesis, cell proliferation and death pathways [8,9]. Therefore, copper-related nanoagents open a new horizon for the development of copper in cancer therapy [10]. However, the intracellular copper is maintained at an extraordinarily low level by active homeostatic mechanisms [11]. Meanwhile, the lack of tumor selectivity is one of the major challenges. Comparatively, nanoagents preferentially accumulate in tumor tissues and can be functionalized with active targeting group to reduce the undesired off-target effects. Thereby, the development of copper delivery nanoagents is highly significant for tumor therapy. Copper has two main valence states Cu^{2+} and Cu^{+}. The oxidation state Cu^{2+} can be reduced to Cu^{+} by the action of glutathione (GSH) reduction. Then, Cu^{+} can be catalyzed by H_2O_2 to produce the toxic •OH through Fenton-like reaction [12,13]. The reaction rate of Cu^{+} is 1×10^4 L mol^{-1} s^{-1}, which is about 158 times than that of Fe^{2+} (~63 L mol^{-1} s^{-1}) [14–16]. Shi *et al.* proposed that the structure of mesoporous silica nanoparticles (Si-O-Si) is adjustable, which can incorporate Fe, Cu, Mg, Ca and other metal elements into its structure under hydrothermal conditions [17–19]. Such a structure can benefit the degradation and release of the metal ions at a specific location, and achieve the

* Corresponding authors.
E-mail addresses: tl8687@163.com (Z. Tang), whzhdicpwtg@dicp.ac.cn (H. Wei), kdyang@zjsru.edu.cn (K. Yang), xywjj2008@163.com (J. Wang).

https://doi.org/10.1016/j.cclet.2024.109742
1001-8417/

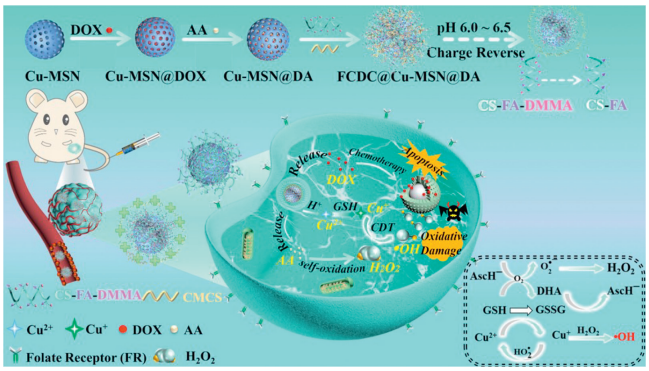

Scheme 1. Schematic illustration of the fabrication process of FCDC@Cu-MSN@DA for active-transporting with charge reversal property and its application for synergistic chemo-chemodynamic therapy.

ideal antitumor effect as a drug delivery system. Compared with normal tissue, tumor tissue is a weak acidic environment, and has relatively high H_2O_2 level to ensure CDT specificity [20–22]. However, the endogenous H_2O_2 as an important substrate for Fenton reaction was still insufficient, which leads the insufficient ROS production and even promotes tumor growth [23]. In order to increase the level of H_2O_2, a variety of nanoagents for H_2O_2 generation have been designed and developed [24–26]. Ascorbic acid (AA) has been involved in many applications in the field of biology [27,28]. Intravenous administration of AA in the range of pharmacologically safe dose (0.3–20 mmol/L) exhibits selective killing effect by producing exogenous H_2O_2 on tumor cells through autoxidation without damaging normal cells [29–31]. The production of H_2O_2 by AA remains at a slow rate through autoxidation reaction (6×10^{-7} s^{-1}) [32], which can be accelerated by the introduction of transition metal catalyst [33–35]. Many researchers have found that AA exhibits pro-oxidation activity in the presence of transition metal copper [36–38]. Meanwhile, the transition metal also induced AA autoxidation to produce H_2O_2 [39,40]. Shi *et al.* [19] designed AA loaded Fe^{3+} doped hollow mesoporous silica nanoagents, which promoted the autoxidation reaction of AA in tumor tissue and enhanced H_2O_2 productivity to enhance the Fenton reaction, leading to severe oxidative damage and more apoptosis of tumor cells.

Herein, a Cu(II)-doped MSNs is developed for enhanced chemodynamic therapy (Scheme 1). DOX and AA are loaded into Cu-MSN, which is further modified with folate acid (FA) functionalized chitosan-maleic anhydride (FA-CS-DMMA) to endow them with prolonged blood circulation and active-transporting ability. Then, the negatively charged hydrophilic chain segment carboxymethyl chitosan (CMC) is coated to endow them with charge reversal ability, resulting in a kind of versatile nanoagents FA-CS-DMMA/CMC@Cu-MSN@DOX/AA(FCDC@Cu-MSN@DA). The resultant FCDC@Cu-MSN@DA can efficiently deliver cargoes into tumor cells by FA active-transporting and charge reversal ability. When FCDC@Cu-MSN@DA reached the tumor tissue, the carboxyl group of CMC was protonated, and the β-carboxylic acid amide bond between DMMA and CS (CS-DMMA) was breaking under the tumor extracellular microenvironment (pH 6.8). Then, the surface charge of nanoagents inverted from negative to positive, which increased the intracellular uptake. The acidic intracellular microenvironment triggered the biodegradation of Si-O-Cu, which accelerated the self-oxidation process of AA to provide more exogenous H_2O_2. Meanwhile, the release of Cu^{2+} was reduced to Cu^{+} by GSH, followed by Fenton-like reaction with exogenous H_2O_2 to produce more toxic hydroxyl radicals ($^{\bullet}OH$), resulting in serious oxidative damage to tumor cells. The *in vitro* and *in vivo* experiments suggested FCDC@Cu-MSN@DA can efficiently inhibit the growth of breast cancer *via* chemo/chemodynamic combination therapy by enhancing oxidative damage.

Cu^{2+} was directly doped into mesoporous silica nanoagents (MSNs) by hydrothermal method. Cetyl trimethylammonium bromide (CTAB) was used as a structural-directing agent in a weakly alkaline ammonia solution in a hydrothermal environment. Cu-MSN was synthesized by the condensation reaction of the silicon dioxide precursor ethyl orthosilicate (TEOS). Then, APTES was added to coordinate with the surface of Cu-MSN. According to transmission electron microscope (TEM) images (Figs. S1A, S2B and S2C in Supporting information) and scanning electron microscopy (SEM) images (Figs. S1C and S2A in Supporting information), Cu-MSN nanoagents were about 50 nm in size with monodispersed spherical morphology, and a clearly visible mesoporous structure through the entire particle. Brunauer-Emmett-Teller (BET) analysis showed that the surface area of Cu-MSN was about 704.71 m^2/g with a mesopore size of 4.5 nm (Fig. S4 in Supporting information). The obtained Cu-MSN showed a hydrodynamic particle size of 105.1 nm by dynamic light scattering (DLS) (Fig. S1F in Supporting information), which further featured a larger hydrodynamic particle size of 213.3 nm after surface coating of FA-CS-DMMA and CMCs (Fig. S1G in Supporting information). The X-ray diffraction (XRD) pattern of Cu-MSN showed that the characteristic peak can ascribe to the amorphous MSN (Fig. S5 in Supporting information). In addition, the small angle XRD patterns showed that both MSN and Cu-MSN exhibited obvious diffraction peak at 2°, which indicated the ordered mesoporous structure in Cu-MSN [24,41]. The selected area electron diffraction (SAED) (Fig. S6 in Supporting information) and XRD results demonstrated the weak crystallization of Cu-MSN. The high-angle annular dark-field scanning TEM (HAADF-STEM) image and corresponding energy dispersive spectrometer (EDS) elemental mappings of Cu-MSN suggested that C, N, O, Si and Cu elements were homogeneously distributed (Fig. S1E in Supporting information). According to the full speactra by X-ray photoelectron spectroscopy (XPS). Cu-MSN showed peaks assigned to C, N, O, Si and Cu (Fig. S1H in Supporting information). The binding energies at 400.1 and 402.3 eV of the N 1s are corresponding to the pyridinic N and graphitic N (Fig. S1I in Supporting information). The O 1s spectrum can be fitted by three peaks at binding energies of ~532.6, 533.2, and 533.5 eV (Fig. S1J in Supporting information). The high-resolution XPS profiles (Fig. S1K in Supporting information) of Cu $2p_{3/2}$ (933.5 eV), Cu $2p_{1/2}$ (953.1 eV), and two strong Cu^{2+} satellites at 962.6 eV and 943.8 eV showed that the consistence of Cu^{2+} in Cu-MSN, which ensured that the release of Cu^{2+} from Cu-MSN nanoagents in acidic conditions to scavenger GSH, thus amplifying the accumulation ROS. TEM and SEM images showed that the prepared FCDC@Cu-MSN@DA were monodispersed with spherical structure (Figs. S1B, S1D and S3 in Supporting information). The amount of Cu^{2+} in FCDC@Cu-MSN@DA 3.3% was determined by inductively coupled plasma-optical emission spectroscopy (ICP-OES).

As a drug delivery system, MSN can transport antitumor drugs to the tumor site. Therefore, it is necessary to design and control the “open” and “close” of the pores under specific stimuli [42]. Compared with normal tissue (pH 7.4), tumor tissue has a weak acidic extracellular environment (pH 6.5–6.9) and endosome (pH 5.0–5.5). The charge reversal ability FCDC@Cu-MSN@DA could enhance the cellular uptake and controlled drug release of MSN [43,44]. Chitosan is a kind of natural cationic polysaccharide with excellent degradability and biocompatibility. The abundant amino groups on the main chain segment of chitosan make it easy to introduce functional groups [45,46]. The FA-CS-DMMA was synthesized according to previous literatures [47,48], and characterized by infrared spectroscopy (Fig. S7 in Supporting information). All the characteristic peaks of chitosan located at 3433 cm^{-1} (OH

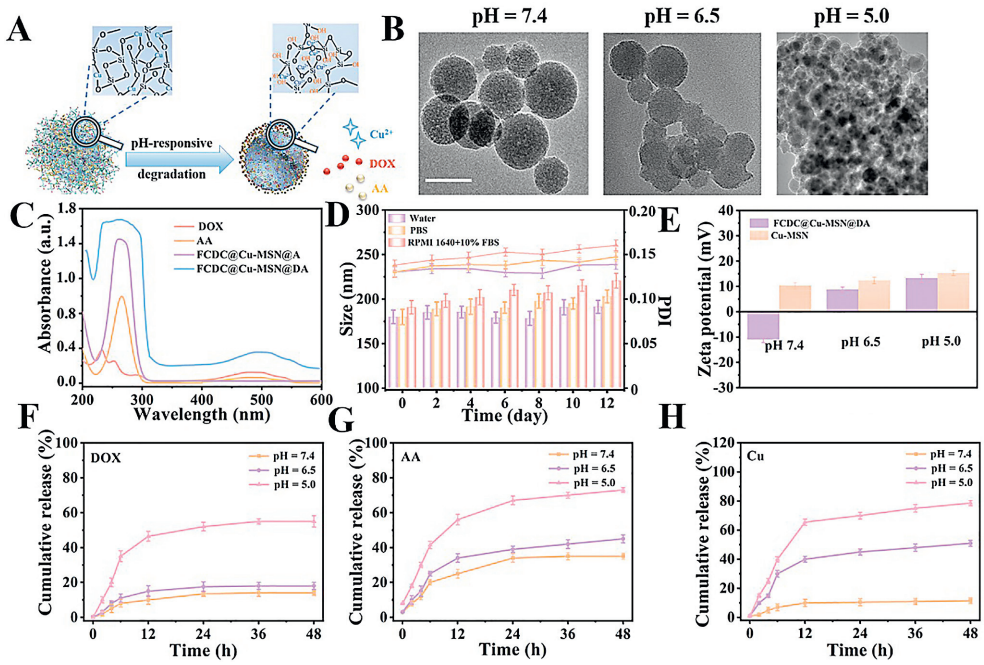

Fig. 1. (A) Schematic diagram of degradation and release of Cu^{2+}, DOX, AA from FCDC@Cu-MSN@DA structure triggered by pH response. (B) TEM images of FCDC@Cu-MSN@DA after immersing with different pH buffer solution (pH 7.4, 6.5, 5.0) for 12 h. Scale bars: 100 nm. (C) UV–vis spectra of DOX, AA, FCDC@Cu-MSN@A, FCDC@Cu-MSN@DA. (D) Size distribution analysis of FCDC@Cu-MSN@DA incubated in water, PBS buffer solution, cell culture medium (RPMI 1640 supplemented with 10% FBS) for 12 days. (E) Zeta potentials of Cu-MSN, FCDC@Cu-MSN@DA in different pH environment (pH 7.4, 6.5, 5.0). (F–H) DOX, AA and Cu^{2+} release from FCDC@Cu-MSN@DA in different pH buffer solution. Data expressed as mean ± standard deviation (SD) ($n = 3$).

stretch), 2869 cm^{-1} (CH stretch), 1618 cm^{-1} (NH bending), 1152 cm^{-1} (stretch of O bridges) and 1078 cm^{-1} (C-O stretch). Chitosan modified folic acid showed various peaks at 1438, 1538, 2850 cm^{-1} corresponding to FA molecule. Specifically, there are major spectral shifting and intensity variations for the chitosan amide I band at 1610–1618 cm^{-1} (mainly ascribed C-O stretch) and amide II band at 1477–1489 cm^{-1} (C=N stretching coupled with N=H bending modes). The intensity variations in the difference spectra of the polymer amide I and amide II bands are due to the acid bindings to chitosan C-O, C=N and N=H groups [49,50]. ^1H NMR was performed to prove the conjugation of FA-CS-DMMA (Fig. S8 in Supporting information). The new signals at δ1.7–1.8 ppm were to the methyl protons of DMMA. The characteristic peaks at 8.48 (a), 7.59 (c), 6.62 (d), 4.22 (b) ppm were assigned to FA. These results strongly indicated the successful synthesis of FA-CS-DMMA copolymer.

As shown in Fig. 1A, Cu-doped MSN can be degradated under acidic environment. TEM images (Fig. 1B) of FCDC@Cu-MSN@DA after different treatments showed that it remained stable after 12 h incubation at pH 7.4. The nanostructure of FCDC@Cu-MSN@DA had markedly partial aggregated after 12 h incubation at pH 6.5. FCDC@Cu-MSN@DA has gradually degraded at pH 5.0 after 12 h. At the same time, the charge reversal ability occurred in different periods of buffer solution. In the weak extracellular acidic environment of tumor (pH 6.0–6.5), due to the protonation and deprotonation of carboxymethyl chitosan and the hydrolytic fracture of β-carboxylic acid amide bonds formed between DMMA and CS (CS-DMMA) [51,52], the surface charge of outer shell inverted from negative to positive. The potential of the nanoagents converted from −10.97 mV to +8.73 mV and even +19.49 mV (pH 5.0) (Fig. 1E). DOX and AA can be loaded simultaneously into MSN due to the large surface area and pore volume of Cu-MSN. BET analysis showed that surface area of FCDC@Cu-MSN@DA was about 178.244 m^2/g in Fig. S4 (Supporting information). The characteristic peaks of AA and DOX in FCDC@Cu-MSN@DA were detected by UV spectrophotometer at 265 nm and 480 nm, respectively (Fig. 1C). The drug loading contents of DOX and AA were 17.65% and 34.4%, respectively. FCDC@Cu-MSN@DA is stable in nearly neutral physiological environment, and it was dispersed in deionized water, phosphate buffer saline (PBS), cell culture medium (RPMI 1640 supplemented with 10% fetal bovine serum (FBS)) to evaluate the changes of particle size over 12 days. The size measured by DLS was about 165 nm and polymer dispersity index (PDI) = 0.15, reflecting the good dimensional stability (Fig. 1D). In the weak acidic microenvironment of tumor tissue, it is easy to break the Cu-O bond [46]. The SAED image of Cu-MSN showed a tendency to weakly crystallize in Fig. S6. SAED and XRD patterns indicated that the frame structure has the possibility of degradation [19], which means the structural collapse. FCDC@Cu-MSN@DA was treated with buffers simulating normal and tumor tissue for 12 h to observe the release of Cu^{2+}, DOX, and AA. According to Fig. 1F, DOX was released more rapidly at pH 5.0 compared to pH 7.4 and pH 6.5. The release of AA was obtained by the UV absorption peak at 265 nm, and 69.7% of AA was released after 24 h in ABS (pH 5.0) buffer (Fig. 1G). The release behaviour of Cu^{2+} detected by ICP-OES was similar to DOX and AA within 24 h (Fig. 1H). In detail, the structure of FCDC@Cu-MSN@DA remains stable in the neutral environment, and the release amount of Cu^{2+} was no more than 10% after 3 days. However, as the structure collapsed obviously in the acidic environment, the release of Cu^{2+} reached nearly 80% after 24 h incubation.

Glutathione is a rich endogenous antioxidant in tumor cells, which can maintain the intracellular redox balance and avoid ROS induced oxidative damage. To demonstrate the GSH depletion capacity of FCDC@Cu-MSN@DA, Ellman's reagent [5,5′-dithiobis(2-nitrobenzoic acid) (DTNB)] was selected as an indicator to assess the residual thiol species according to the colored TNB (5-mercapto-2-nitrobenzoic acid) species formation (Fig. S9A in Supporting information). As revealed in Fig. S9C (Supporting in-

formation), the absorbance intensity of TNB at 412 nm decreased obviously with the increase of time, meanwhile, the yellow color solutions gradually weakened, which indicated that Cu^{2+} has a strong ability to consume GSH. However, the DTNB method is a conceptual approach that is insufficient to quantify the consumption of GSH. The consumption of GSH and the formation of GSSG can be demonstrated by ^{1}H NMR [53]. As shown in Fig. S9B (Supporting information), after 24 h incubation with FCDC@Cu-MSN@DA, the characteristic chemical peaks of GSH (δ4.57 ppm, Cys-CH; 2.84 ppm, Cys-CH_2) disappeared. Meanwhile, the new peaks (δ3.25 ppm, Cys-CH_2; 3.17 ppm, Cys-CH_2) matched with the characteristic signals of GSSG appeared. Electron spin resonance (ESR) spectrometry was further employed to confirm the catalytic functionality of the nanoagents and the generation of $^{\bullet}$OH. 5,5-Dimethyl pyridine *N*-oxide (DMPO) was selected as a spin-trap agent that mixed with AA, Cu-MSN+AA, FCDC@Cu-MSN@A, FCDC@Cu-MSN@DA, respectively (Fig. S9D in Supporting information). Characteristic signal of $^{\bullet}$OH (1:2:2:1) was detected by ESR spectrum of FCDC@Cu-MSN@A and FDCD@Cu-MSN@DA groups in acidic H_2O_2 solution, while no signal was detected in AA group, demonstrating the highly catalytic activity of FCDC@Cu-MSN@A and FDCD@Cu-MSN@DA to produce $^{\bullet}$OH. Studies have shown that DOX can produce H_2O_2 [44]. When DOX and AA provide H_2O_2 at the same time, CDT can be strongly enhanced. These results suggested that with the decomposition of FCDC@Cu-MSN@DA under the acidic environment, it can self-supply exogenous H_2O_2 by DOX and AA to enhance the level of toxic $^{\bullet}$OH. Fig. S9E (Supporting information) showed with the extension of the catalytic reaction time, the generation of $^{\bullet}$OH is significant time-dependent. The generation ability of $^{\bullet}$OH by FCDC@Cu-MSN@DA was then evaluated by using the 3,3′,5,5′-tetramethylbenzidine (TMB) assay. TMB can be oxidized by $^{\bullet}$OH to produce a deep blue color in acidic condition with maximum absorbance at 370 nm [54]. As shown in Fig. S9F (Supporting information), FCDC@Cu-MSN@DA nanoagents reacted with TMB in neutral and alkaline conditions showed no obvious color change, comparatively, it caused an apparent color change under mild acidic (pH 5.0) condition. Cu^{2+} and H_2O_2 led to a rapid color change in TMB aqueous solution. As shown in Fig. S9G (Supporting information), FCDC@Cu-MSN@DA reacted with TMB in an acid environment (pH 5.0), and the solution appeared distinctly blue. H_2O_2 can be produced by AA through self-oxidation, which enhanced Cu^{2+} induced Fenton-like reaction (Fig. S9H in Supporting information). The fading reaction of methylene blue (MB) could also be used for the detection of $^{\bullet}$OH (Figs. S10 and S11 in Supporting information). Time-dependent ultraviolet–visible spectroscopy (UV–vis) absorption spectra of MB contained Cu-MSN solution (1 mg/mL) placed in the presence/absence of AA at pH 5.0 or 7.4, respectively. In acidic solution, Cu^{2+} in Cu-MSN reacted with H_2O_2 produced by AA auto-oxidation to produce $^{\bullet}$OH. Meanwhile, UV absorption peak intensity of MB at 664 nm was weakened.

The transportation efficiency and the degree of cell internalization are the critical factors to determine the therapeutic effect. Folic acid is widely used as a targeted recognition molecule in drug delivery systems (DDS). Folate modified nanoparticles enter tumor cells mainly by binding to the overexpressed folate receptors on the surface of cancer cells, forming complexes, and then entering cancer cells through internalization. Breast cancer cell (MCF-7, 4T1) lines are common folate receptor overexpressed cell lines. Here, Bio-TEM was used to investigate the internalization of FCDC@Cu-MSN@DA by 4T1 cells for different times (Fig. S12 in Supporting information). Compared with non-targeted group CDC@Cu-MSN@DA, cells treated with active-transporting FCDC@Cu-MSN@DA manifested more intracellular internalization. As time increased, more and more gray-black nanoagents were appeared in the vesicles in 4T1 cells by FCDC@Cu-MSN@DA.

Confocal laser scanning microscopy (CLSM) analysis was performed for different cells to further investigate the effects of FA ligands on the cellular uptake. The images evidenced that FA conjugation markedly increased the cellular uptake of FCDC@Cu-MSN by folic acid receptors (FR)-positive cells (MCF-7 and 4T1 cells), compared with FR-negative A549 cells (Fig. S13A in Supporting information). The red fluorescence of DOX in 4T1 cells shows significantly time-dependent behavior of cellular uptake (Fig. S13B in Supporting information).

MTT assay was adopted to detect the cytocompatibility of blank Cu-MSN and FCDC@Cu-MSN on EC and 4T1 cells. As shown in Fig. S13C (Supporting information), the cell viability of normal cells was not affected by Cu-doped nanoagents at various concentrations (20–200 μg/mL) within 24 h, due to the lack of conditions to catalyze the Fenton-like reaction, indicating the good cytocompatibility of Cu-doped nanoagents *in vitro*. Cu-MSN and FCDC@Cu-MSN alone showed negligible toxicity to 4T1 cells (Fig. S13D in Supporting information), even at concentrations up to 200 μg/mL. We investigated the therapeutic effect of different nanoagents by MTT assay and living/dead cell staining assay. We found that the therapeutic effects of all groups were copper-dependent. As displayed in Fig. S13E (Supporting information), free DOX and FCDC@Cu-MSN@A manifested limited killing efficacy on 4T1 cells. When DOX was combined with CDT (CDC@Cu-MSN@DA, FCDC@Cu-MSN@DA), which had an enhanced inhibitory effect on 4T1 cells. Expectedly, due to the higher internalization of active-transporting FCDC@Cu-MSN@DA by 4T1 cells, FCDC@Cu-MSN@DA could more efficiently kill 4T1 cells, and cell viability was less than 20%. The results of live/dead cell staining and semi-quantification of fluorescence (Figs. S13F and G in Supporting information) showed that the targeted group FCDC@Cu-MSN@DA showed stronger red fluorescence compared to the monotherapy and non-targeted groups. The oxidation of ascorbic acid followed by Cu^{2+} release enhanced the Fenton reaction efficacy and chemotherapy. Meanwhile, the superior killing effect of FCDC@Cu-MSN@DA was also supported by living/dead cell staining assay of MCF-7 and A549 cells (Figs. S14 and S15 in Supporting information), wherein FCDC@Cu-MSN@DA group exhibited the smallest number of live MCF-7 cells. The viability of A549 cells treated by FCDC@Cu-MSN@DA group was much higher than those of MCF-7 and 4T1 cells at the same concentration of drug, due to the higher internalization of FCDC@Cu-MSN@DA by 4T1 and MCF-7 cells.

Mitochondria dysfunction such as mitochondrial morphological change, volume shrinkage, membrane potential loss and other characteristics could also lead to cell apoptosis. The mitochondrial damage was evaluated by monitoring its membrane potential change with JC-1 as a fluorescent probe, which displays red fluorescence (JC-1 aggregates) in normal mitochondria but tends to emit green fluorescence (JC-1 monomers) in dysfunctional mitochondria. As shown in Fig. 2A, the cells treated with FCDC@Cu-MSN@DA group displayed the strongest green/red influence intensity ratio, suggesting the serious mitochondria dysfunction. The semiquantitative analysis of the fluorescence intensity of aggregation of 4T1 cells was shown in Fig. 2B. Meanwhile, 2,7-dichlorofluorescin diacetate (DCFH-DA) probe as a chemical probe to evaluate the intracellular ROS level (Fig. 2C and Fig. S16 in Supporting information). Compared with other groups, the cells treated with FCDC@Cu-MSN@DA showed the strongest green fluorescence intensity, which resulted from the increased H_2O_2 level produced by AA and GSH depletion.

GSH is highly involved in cuproptotic, ferroptotic and apoptotic cell death. The GSH-depletion efficiency was evaluated by the GSH-GSSG assay kit (Fig. 2D). As except PBS, all other groups including FCDC@Cu-MSN@D, FCDC@Cu-MSN@A, CDC@Cu-MSN@DA and FCDC@Cu-MSN@DA could drastically scavenge intracellular GSH. It

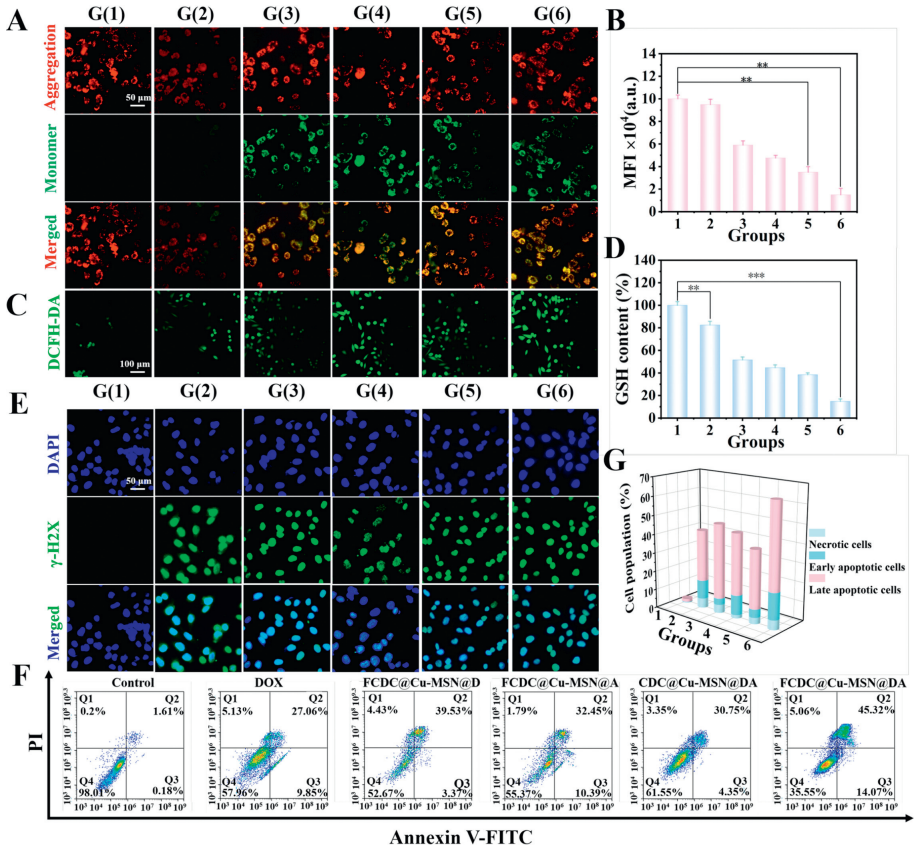

Fig. 2. (A) CLSM images of the mitochondrial membrane potential stained with JC-1 probe in 4T1 cells after different treatments. Scale bar: 50 μm. (B) The semiquantitative analysis of the fluorescence intensity of aggregation of 4T1 cells. (C) CLSM images of 4T1 cells stained with DCFH-DA probe showing the GSH level and (D) the semiquantitative analysis of intracellular GSH content after different treatments. Scale bar: 100 μm. (E) CLSM images of DNA damage of 4T1 cells treated with different formulations. (F) Flow cytometry assay of 4T1 cells after different treatments. Scale bar: 50 μm. (G) Population of early apoptotic, late apoptotic and necrotic 4T1 cells induced with various treatments. G(1): PBS; G(2): DOX; G(3): FCDC@Cu-MSN@D; G(4): FCDC@Cu-MSN@A; G(5): CDC@Cu-MSN@DA; G(6): FCDC@Cu-MSN@DA. Data are presented as mean ± SD ($n = 4$). $^{**}P < 0.01$, $^{***}P < 0.001$.

was noted that there was no significant difference in GSH depletion, due to the reduction of Cu^{2+} to Cu^{+} with the consumption of GSH. The content of GSH in DOX) treated cells slightly reduced, which was probably due to the DOX produces oxidizing substance H_2O_2.

DNA can be damaged by oxidation, resulting in mitochondrial dysfunction and changes in mitochondrial membrane permeability. The level of γ-H2AX can clearly reflect the degree of DNA damage and repair, and has been widely used in the study of DNA damage and apoptosis. DOX has strong cytotoxic effects by destroying the DNA double strand in the tumor nucleus. DNA damage assay kit is used to assess DNA damage of the nucleus in 4T1 cells. Predictably, except PBS group, the other groups showed obvious green fluorescence, indicating significant DNA damage (Fig. 2E). Cell apoptosis was evaluated by flow cytometry at different treatments using AnnexinV-FITC and PI Apoptosis Detection kit. As shown in Figs. 2F and G, the apoptotic ratio of cells treated with DOX was only 36.91%, while other in FCDC@Cu-MSN@D, FCDC@Cu-MSN@A and CDC@Cu-MSN@DA groups were 42.9%, 48.84% and 35.1%, respectively. Notably, the greatest therapeutic efficacy was observed in FCDC@Cu-MSN@DA group, and the cell apoptosis rate was as 59.39%.

To visualize the distribution of nanoagents *in vivo*, FCDC@Cu-MSN@DA and CDC@Cu-MSN@DA were injected into 4T1 tumor-bearing BALB/c mice. The animal experiments were approved by the Institutional Animal Care and Use Committee of Chengdu Medical College and performed in compliance with the guidelines. Then, DOX influence intensity at different time intervals and different sites were monitored. Compared with non-targeted group, FA-targeted group FCDC@Cu-MSN@DA was accumulated at the tumor site more obviously, and DOX fluorescence intensity reached the maximum value at 24 h in Fig. S17A (Supporting information). *Ex vivo* imaging showed that the non-targeted group CDC@Cu-MSN@DA was distributed to the normal sites rather than to the tumor site. In contrast, only a little of the charge-reversal targeted FCDC@Cu-MSN@DA nanoagents were aggregated at the normal tissues, much more were accumulated at the tumor site (Fig. S17B in Supporting information). These images suggested that targeted group FCDC@Cu-MSN@DA showed much better selectivity *in vivo*.

The antitumor efficacy of different nanoagents was further evaluated in 4T1 tumor-bearing BALB/c mice (Fig. 3A). As shown in Fig. 3B, minimal side effect was observed. Treatment with either free DOX, FCDC@Cu-MSN@D or FCDC@Cu-MSN@A alone showed little anti-tumor activity (Figs. 3D and E). The tumor tissues treated by FCDC@Cu-MSN@DA group gradually shrank after 4 times injections. The results of relative tumor volume after 14 days treatment demonstrated that FCDC@Cu-MSN@DA group showed 90.4% tumor inhibition (Fig. S18 in Supporting information), markedly higher than FCDC@Cu-MSN@D (71.6%) and FCDC@Cu-MSN@A (69.2%). Tumor weight was markedly suppressed by FCDC@Cu-MSN@DA group with chemo/chemodynamic therapy (Fig. 3F). The corresponding hematoxylin and eosin (H&E) staining, terminal deoxynucleotidyl transferase dUTP nick end labeling (TUNEL) staining and Ki67 staining on tumor tissues showed that FCDC@Cu-MSN@DA group achieved maximum tumor necrosis and apoptosis (Fig. 3C). These results indicated that the excellent anti-tumor

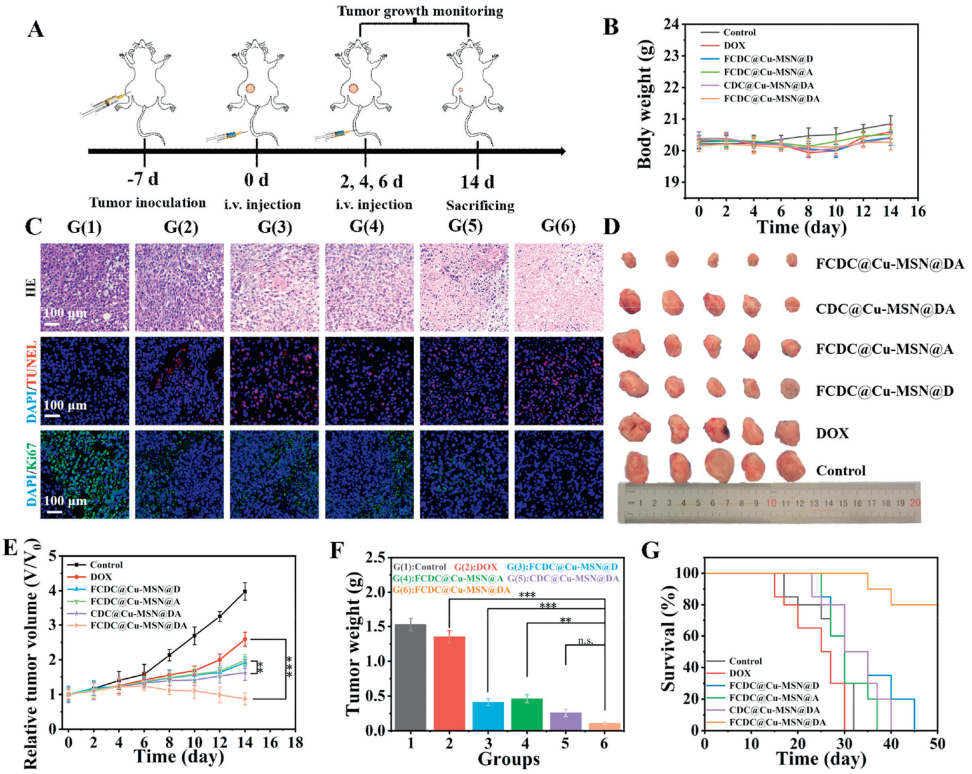

Fig. 3. *In vivo* anti-tumor effect ($n = 6$ per group). (A) Schematic illustration of tumor model establishment and treatment process. (B) The biocompatibility was evaluated by body weight changes with different treatments as a function of time. (C) Photos of mice at the end of the experiment, and H&E, TUNEL, and Ki-67 staining of the tumor slices with different treatments after 14 days. Scale bar: 100 μm. (D) Photographs of the resected tumors on the 14th day. (E) Tumor volumes and (F) tumor weight after various treatments. (G) Survival rate of BALB/c mice bearing 4T1 tumor with different treatments. G(1): PBS; G(2): DOX; G(3): FCDC@Cu-MSN@D; G(4): FCDC@Cu-MSN@A; G(5): CDC@Cu-MSN@DA; G(6): FCDC@Cu-MSN@DA. Data are shown as mean ± SD ($n = 5$). *P*-values were calculated using one-way ANOVA with Tukey's *post-hoc* test, ns means no significance. $^{**}P < 0.01$, $^{***}P < 0.001$.

efficiency of FCDC@Cu-MSN@DA group was due to the combination of chemotherapy and chemodynamic therapy. In addition, the biocompatibility was also evaluated. Blood routine and biochemical analysis were performed on the 14th day after different treatment. As shown in Fig. S19 (Supporting information), the liver and kidney function markers were all within the normal value range. H&E staining (Fig. S20 in Supporting information) was conducted to evaluate the histopathological changes in major organs (heart, liver, spleen, lung, and kidney). These assays further suggested that FCDC@Cu-MSN@DA group showed the negligible side effects *in vivo*, and could markedly prolong the survival time of BALB/c mice bearing 4T1 tumor in Fig. 3G.

In conclusion, we successfully synthesized a pH responsive active-transporting nanoagent FCDC@Cu-MSN@DA with charge reversal ability. When FCDC@Cu-MSN@DA nanoagent entered into tumor cells, the degradation of the Si-O-Cu hybrid framework not only induced the release of Cu^{2+} in the acidic environment but also effectively accelerated the oxidation of AA to produce more exogenous H_2O_2. The generated Cu^{2+} converted H_2O_2 into more highly toxic hydroxyl radical (•OH) *via* Fenton-like reaction, thus, accelerating the cell apoptosis by achieving synergistic treatment with enhanced CDT and DOX. The *in vitro* and *in vivo* experiments confirmed that FCDC@Cu-MSN@DA can efficiently inhibit the growth of breast cancer by enhancing oxidative damage *via* chemo/chemodynamic combination therapy. This work provides a new biocatalyst for producing exogenous H_2O_2, which offers a new path for engineering multimodal nanoagents to achieve synergistic inhibition of breast cancer, and inspire diverse novel discoveries in a wide range of therapeutics and biomedical fields.

Declaration of competing interest

The authors declare that they have no known competing financial interests or personal relationships that could have appeared to influence the work reported in this paper.

Acknowledgments

This work was financially supported by the National Key Research and Development Program of China (No. 2019YFA0705803), the National Natural Science Foundation of China Youth Fund (Nos. 51803174, 82102470), the Natural Science Foundation of Sichuan Province (No. 24NSFSC4798) and the Foundation of Sichuan Engineering Technology Research Center of Basalt Fiber Composites Development and Application of Southwest Petroleum University (No. 2022SCXWYXWFC002). We acknowledged the support from the School of New Energy and Materials of Southwest Petroleum University, Sichuan International Science and Technology Cooperation Base, and Dalian Institute of Chemical Physics of Chinese Academy of Sciences.

Supplementary materials

Supplementary material associated with this article can be found, in the online version, at doi:10.1016/j.cclet.2024.109742.

References

[1] A.L.Z. Lee, V.W.L. Ng, S. Gao, et al., Adv. Funct. Mater. 24 (2014) 1538–1550.
[2] Z.M. Tang, W.J. Tian, Mater. Rep. 36 (2022) 21120187-6.

[3] Z.M. Tang, W.J. Tian, Mater. Rep. 37 (2023) 22010219-7.
[4] F.W. Sun, Y.Y. Peng, Y.P. Li, et al., Chin. Chem. Lett. 34 (2023) 107507.
[5] G. Liu, J. Zhu, H. Guo, et al., Angew. Chem. 131 (2019) 18814–18819.
[6] F. Jiang, C.Z. Yang, B.B. Ding, et al., Chin. Chem. Lett. 33 (2022) 2959–2964.
[7] J.X. Xu, J.W. Zhang, J.P. Song, et al., J. Colloid Interface Sci. 628 (2022) 271–285.
[8] W. Xu, Y. Wang, G. Hou, et al., Adv. Healthc. Mater. 12 (2023) e2202949.
[9] S.P. Ning, M. Lyu, M.D. Zhu, et al., ACS Nano 17 (2023) 10206–10217.
[10] T. Peter, C. Shannon, P. Boryana, et al., Science 375 (2022) 1254–1261.
[11] E.J. Ge, A.I. Bush, A. Casini, et al., Nat. Rev. Cancer 22 (2022) 102–113.
[12] Z.M. Tang, S.T. Jiang, Y.D. Wang, et al., Mater. Rep. 37 (2023) 22050131.
[13] B.L. Ma, S. Wang, F. Liu, et al., J. Am. Chem. Soc. 141 (2019) 849–857.
[14] N. Masomboon, C. Ratanatamskul, M.J. Lu, Environ. Sci. Technol. 43 (2009) 8629–8634.
[15] N. Kang, D.S. Lee, Chemosphere 47 (2002) 915–924.
[16] D.A. Nichela, A.M. Berkovic, M.R. Costante, et al., Chem. Eng. J. 228 (2013) 1148–1157.
[17] W.C. Wu, L.D. Yu, Q.Z. Jiang, et al., J. Am. Chem. Soc. 141 (2019) 11531–11539.
[18] B.W. Yang, H.L. Yao, H. Tian, et al., Nat. Commun. 12 (2021) 3393.
[19] B.W. Yang, J.L. Shi, J. Am. Chem. Soc. 142 (2020) 21775–21785.
[20] P. Yu, X.D. Li, G.H. Cheng, et al., Chin. Chem. Lett. 32 (2021) 2127–2138.
[21] D. Trachootham, J. Alexandre, P. Huang, Nat. Rev. Drug Discov. 8 (2009) 579–591.
[22] Z.M. Tang, Y.Y. Liu, M.Y. He, et al., Angew. Chem. 131 (2019) 958–968.
[23] Q.B. Cui, J.Q. Wang, Y.G. Assaraf, et al., Drug Resist. Updat. 41 (2018) 1–25.
[24] S.M. Dong, Y.S. Dong, T. Jia, et al., Chem. Mater. 32 (2020) 9868–9881.
[25] L. Zhao, Z.X. Li, J.J. Wei, et al., Chem. Eng. J. 430 (2022) 133057.
[26] M. Yuan, L.Y. Zhang, T. Ma, et al., ACS Appl. Mater. Interfaces 14 (2022) 15970–15981.
[27] D. Du, J.J. Cullen, G.R. Buettner, Biochim. Biophys. Acta 1826 (2012) 443–457.
[28] M. Giansanti, T. Karimi, I. Faraoni, et al., Cancers 13 (2021) 1428.
[29] E. Campbell, M. Vissers, C. Wohlrab, et al., Free Radic. Biol. Med. 100 (2016) S132.
[30] S. Hercberg, P. Galan, P. Preziosi, et al., JAMA Intern. Med. 164 (2004) 2335–2342.
[31] Q. Chen, M.G. Espey, M.C. Krishna, et al., Proc. Natl. Acad. Sci. U. S. A. 102 (2005) 13604–13609.
[32] K. Linowiecka, M. Foksinski, A.A. Brożyna, Nutrient 12 (2020) 3869.
[33] M.M.T. Khan, A.E. Martell, J. Am. Chem. Soc. 89 (1967) 4176–4185.
[34] R.W. Peterson, J.H. Walton, J. Am. Chem. Soc. 65 (1943) 1212–1217.
[35] J.D. Schoenfeld, M.S. Alexander, T.J. Waldron, et al., Semin. Radiat. Oncol. 29 (2019) 25–32.
[36] S.M. Hadi, M.F. Ullah, U. Shamim, et al., Chemotherapy 56 (2010) 280–284.
[37] S.Q. Zhou, Y.H. Yu, J.L. Sun, et al., Chem. Eng. J. 333 (2018) 443–450.
[38] M.E. Letelier, S.S. Jofré, L.P. Silva, et al., Chem. Biol. Interact. 188 (2010) 220–227.
[39] Y.J. Ai, H. Sun, Z.X. Gao, et al., Adv. Funct. Mater. 31 (2021) 2103581.
[40] S.A. Fahmy, A. Ramzy, A.A. Mandour, et al., Pharmaceutics 14 (2022) 407.
[41] W.J. Xu, T.B. Wang, J.M. Qian, et al., Chem. Eng. J. 437 (2022) 135311.
[42] P. Huang, D.Z. Lian, H.L. Ma, et al., Chin. Chem. Lett. 32 (2021) 3696–3704.
[43] B.X. Ma, W.H. Zhuang, Y.A. Wang, et al., Acta Biomater. 70 (2018) 186–196.
[44] X.B. Zhao, Z.H. Wei, Z.P. Zhao, et al., ACS Appl. Mater. Interfaces 10 (2018) 6608–6617.
[45] M. Dash, F. Chiellini, R.M. Ottenbrite, et al., Prog. Polym. Sci. 36 (2011) 981–1014.
[46] Y.L. Miao, Y.D. Qiu, W.J. Yang, et al., Colloids Surf. B: Biointerfaces 169 (2018) 313–320.
[47] S.J. Yang, F.H. Lin, K.C. Tsai, et al., Bioconjug. Chem. 21 (2010) 679–689.
[48] S.K. Liu, W.T. Li, S.L. Gai, et al., Biomater. Sci. 7 (2019) 951–962.
[49] M.C. Shi, Z.T. Chen, S.B. Farnaghi, et al., Acta Biomater. 30 (2016) 334–344.
[50] S.E. Boroujeni, S.B. Khoulenjani, H. Mirzadeh, et al., Prog. Biomater. 5 (2016) 1–8.
[51] J.Z. Du, H.J. Li, J. Wang, Acc. Chem. Res. 51 (2018) 2848–2856.
[52] Y.N. Du, Y.N. Li, X.Z. Li, et al., Adv. Funct. Mater. 30 (2020) 1904697.
[53] J.B. Aleta, M.S. Albero, J.C. Funes, et al., J. Colloid Interface Sci. 617 (2022) 704–717.
[54] B. Tian, S. Liu, C. Yu, et al., Adv. Funct. Mater. 33 (2023) 2300818.